Observation and analysis of Fano-like lineshapes in the Raman spectra of molecules adsorbed at metal interfaces

S. Dey, M. Banik, E. Hulkko, K. Rodriguez, V. A. Apkarian, M. Galperin, and A. Nitzan

Phys. Rev. B **93**, 035411 — Published 7 January 2016

DOI: 10.1103/PhysRevB.93.035411

Observation and analysis of Fano-like lineshapes in the Raman spectra of molecules adsorbed at metal interfaces

S. Dey,[1] M. Banik,[1] E. Hulkko,[1,2] K. Rodriguez,[1] V. A. Apkarian,[1] M. Galperin,[3] and A. Nitzan[4,5]

[1]*Department of Chemistry, University of California, Irvine, California 92697-2025, USA*
[2]*Depratment of Chemistry, PO Box 35, FI-40014, University of Jyväskylä, Finland*
[3]*Department of Chemistry and Biochemistry, University of California at San Diego, La Jolla, CA 92093, USA*
[4]*Department of Chemistry, University of Pennsylvania, Philadelphia, Pennsylvania 19104, USA*
[5]*School of Chemistry, Tel Aviv University, Tel Aviv, 69978, Israel*

Surface enhanced Raman scattering (SERS) from bipyridyl ethylene adsorbed on gold dumbbells shows Fano-like spectra at high incident light intensity. This is accompanied by an increased electronic temperature, while no vibrational anti-Stokes (AS) scattering is observed. Theory indicates that interference between vibrational and electronic Raman scattering can yield such asymmetric scattering lineshapes. The best fit to observations is obtained by disregarding this coupling and accounting for the detailed lineshape of the continuous electronic component of the SERS.

PACS numbers: 85.65.+h 73.23.-b 78.20.Jq 78.67.-n

I. INTRODUCTION

Surface enhanced optical response of molecules adsorbed on metal surfaces reflects the effect of strong local fields created by surface plasmons[1–3] as well as charge transfer between the molecule and metal.[4–7] Surface enhanced Raman scattering (SERS) has become an important diagnostic tool for molecules at metallic interfaces including molecular conduction junctions.[8–15] (See also Refs. 16–27 for related theoretical work). At metal interfaces, vibrational Raman scattering is accompanied by a continuous background resulting from inelastic contributions of electron-hole (e-h) excitations in the metal.[1,4,28–30] Both components of the inelastic scattering signal were recently used to determine the bias induced heating in a molecular conduction junction.[13]

While it is generally recognized that the electronic background is affected by the molecule-substrate interaction, these two components of the SERS signal are usually treated separately. Surprisingly, we observe (Fig. 1) an apparent Fano-like feature in the Raman spectra from the same system - bipyridyl ethylene adsorbed on gold nanosphere dimers (dumbbells) that may indicate interference between these two scattering channels. Below we discuss the origin of this observation. It should be noted that Fano-like profiles where previously observed[31] in the surface enhanced-femtosecond stimulated Raman spectra of the same system as in the present study - bipyridyl ethylene (BPE) molecules adsorbed on gold nanosphere dimers (dumbbells). This observation was attributed to interference between the vibrational coherence generated by the combined action of pump and probe pulses and plasmons excited in the metal structure. However no detailed mechanism was offered. Such a mechanism should account also for the observed absence of interference effects in the normal Raman scattering from the same system and for the fact that, while coupling between vibrations and metal is needed to account for such interference, no effect of the proximity to the metal on the vibrational decoherence rate could be detected.

The measurements are carried out on single silica encapsulated gold dumbbells (Fig. 1 right inset). The nanosphere diameter is 95 ± 5 nm and the intersphere spacing prior to irradiation is ~ 1 nm. On these dumbbells, the quadrupolar and the binding dipolar plasmon resonances occur near 560 nm and 780 nm, respectively.[32] As molecular reporter, BPE is adsorbed on the gold

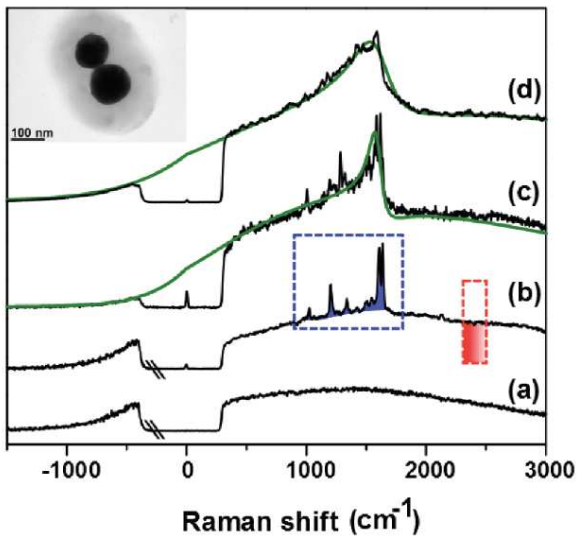

FIG. 1: Raman spectrum recorded on (a) a bare dumbbell, without reporter molecules at low irradiation intensity ($\sim$ 10 μW/μm^2); (b) with reporter molecules at the same low intensity; (c) and (d) with reporter molecules at irradiation intensities $\sim$ 50 μW/μm^2 and $\sim$ 150 μW/μm^2, respectively. Demarcations on (a) and (b) indicate a magnification of the anti-Stokes (AS) region (7x and 4.5x, respectively). The green traces overlapping the (c) and (d) lines are fits to the Fano lineshape (see SI). The blue and red rectangles are used to quantify the intensity dependence of the molecular lines (blue) and electronic Raman scattering of gold (red). The latter leads to results shown in Fig. 2.

spheres prior to encapsulation. The dumbbells are dispersed on a silicon nitride membrane (20 nm thick) of a TEM grid by drop casting them in a dilute solution. Locations and geometries of the nanostructures are mapped using a scanning electron microscope (SEM), then Raman scattering measurements are done under an optical microscope, in the backscattering geometry, using an objective with a numerical aperture of NA = 0.625. The excitation source is a continuous wave diode laser, operating at $\lambda = 532$ nm, coincident with the anti-bonding quadrupolar surface plasmon resonance.[32] The molecular vibrational Raman spectra appear over a background continuum (Fig. 1b), which is also seen on bare dumbbells (Fig. 1a). As discussed before,[33] at low intensity, 10 μW/μm^2, the vibrational spectrum is not affected by the proximity to the metal (in agreement with Ref. 31) and matches that of the isolated BPE molecule. Two observations are most significant at higher incident intensities: (a) The molecular lines broaden asymmetrically to eventually coalesce into the single asymmetric profile, similar to Fano-type lineshape (Figs. 1c and d). (b) The electronic and vibrational temperatures, T_e and T_v, inferred from the AS branch of the electronic Raman scattering (see Fig. 2) and S/AS intensity ratio of the vibrational Raman line appear to be different. At the highest incident light intensity T_e reached 580 K, while no molecular AS scattering is seen, which would set the apparent vibrational temperature of the molecule, T_v, to less than 300 K. More experimental details and results are presented in the SI.

The central question raised by these observations is whether the lineshapes shown in Figs. 1c, d are indeed interference features as their Fano-like lineshapes suggest. Specifically: can there be interference between the electronic and vibrational Raman scattering pathways that coexist in this system? The intuitive answer is negative, because the two pathways lead to different final states. In contrast, in this paper we present theoretical models that show that such interference can happen. Our theory focuses on the generic aspects of such processes, and yields two main results: (a) The aforementioned interference can exist in the presence of electron-vibration coupling and can in principle lead to the observed lineshapes. (b) However, comparing the detailed calculations with the available experimental observations suggests that another mechanism, asymmetric electronic sidebands dressing the molecular Raman spectrum, may be dominant in this system.

We consider two models, described in Section II. One of these (Model A) assumes that the dominant optical interaction is intramolecular and that the effect of the metal substrate results from the molecule-metal interaction. Model B considers, in addition to the intramolecular optical processes, also optically induced molecule-metal charge transfer. Section III and the SI describe our theoretical approach and Section IV presents the results of our model calculations. Section V concludes.

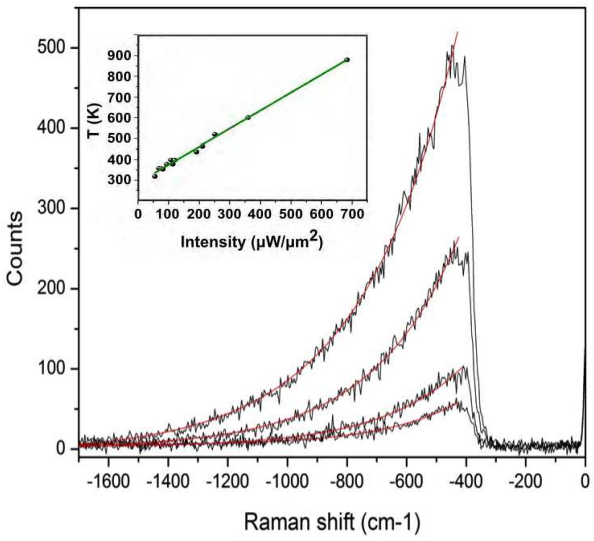

FIG. 2: The anti-Stokes branch of the continuum is given by the thermal occupation of the Fermi-Dirac distribution. This is illustrated by the exponential fits, $I_{AS}(\mathcal{E}) = \exp(-\mathcal{E}/kT_e)$, to the anti-Stokes continuum for four different irradiation intensities, $I = 100, 50, 25, 13$ μW/μm^2, which yield electronic temperatures of $T_e = 465, 415, 395, 364$ K, respectively. A more accurate value of T_e is obtained from fitting to Eq. (S1), but the trend does not change.The inset shows a TEM image of a typical dumbbell. The left inset shows the temperature extracted from the fit of the AS branch of the electronic Raman spectrum (continuum) to the Fermi Dirac distribution. No vibrational AS signal is detected.

II. MODELS

We consider a molecule chemisorbed on a metal surface and subjected to an external radiation field. In the experimental system the metal is a nanostructure (NS) that promotes plasmonic enhancement, but this enters our discussion only implicitly, through the magnitude of the local electromagnetic field. The model Hamiltonian comprises the molecule, metal, radiation field and their couplings, with the electron-photon and e-v interaction terms treated as perturbations:

$$\hat{H} = \hat{H}_0 + \hat{V}_{rad} + \hat{V}_{e-v} \tag{1}$$

where ($\hbar = k_B = e = 1$)

$$\hat{H}_0 = \hat{H}_M + \hat{H}_{NS} + \hat{V}_{NS} + \hat{H}_{rad}; \tag{2}$$

$$\hat{H}_M = \sum_{m=g,x} \varepsilon_m \hat{d}_m^\dagger \hat{d}_m + \omega_v \hat{v}^\dagger \hat{v}; \tag{3}$$

$$\hat{H}_{NS} = \sum_k \varepsilon_k \hat{c}_k^\dagger \hat{c}_k; \tag{4}$$

$$\hat{V}_{NS} = \sum_{m=g,x} \sum_k \left(V_{mk} \hat{d}_m^\dagger \hat{c}_k + V_{km} \hat{c}_k^\dagger \hat{d}_m \right); \tag{5}$$

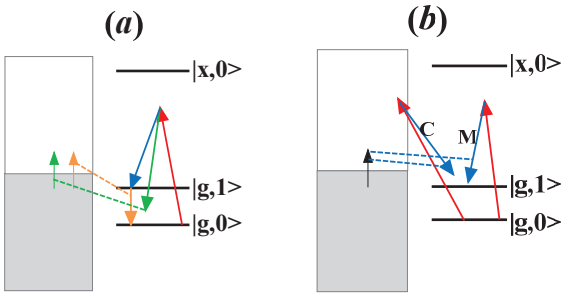

FIG. 3: (Color online) A sketch of the processes underlying the Stokes (S) component of Raman scattering from a molecule coupled to a metal. (a) The incident photons induce the virtual transition (red) and a corresponding Rayleigh scattering (the red process in reverse). In addition two inelastic scattering (Raman) pathways are shown: electronic Raman scattering (green), which brings the molecule to its ground state while creating an e-h excitation in the metal, and vibrational Raman scattering (blue), which brings the molecule to an excited vibrational state on the electronic ground state. These Raman scattering pathways are coupled by the combined effect of the metal-molecule electron transfer and the electronic-vibrational (e-v) interaction (orange) that induces vibrational de-excitation in the molecule with e-h formation in the metal (dashed lines). (b) Two pathways are defined by the excitation process (red): a virtual molecular transition (M) and a molecule-to-metal charge transfer transition (C). The outgoing photon (blue) leaves the molecule in the excited vibrational state, possibly with e-h (de-)excitation in the metal (black). The processes shown are accompanied also by electronic Raman scattering from the bare metal.

$$\hat{V}_{e-v} = \sum_{m=g,x} M_m \hat{Q}_v \hat{d}_m^\dagger \hat{d}_m; \hat{Q}_v = \hat{v} + \hat{v}^\dagger \tag{6}$$

$$\hat{H}_{rad} = \sum_{\alpha\in i,\{f\}} \nu_\alpha \hat{a}_\alpha^\dagger \hat{a}_\alpha; \tag{7}$$

$$\hat{V}_{rad} = \hat{V}_{rad}^C + \hat{V}_{rad}^M \tag{8}$$
$$= \sum_{J=C,M} \sum_{\alpha\in i,\{f\}} \left(U_{gx,\alpha}^J(\hat{Q}_v) \hat{D}_J^\dagger \hat{a}_\alpha + U_{\alpha,gx}^J(\hat{Q}_v) \hat{a}_\alpha^\dagger \hat{D}_J \right)$$

$\hat{H}_M$ is the molecular Hamiltonian, modeled as a two electronic levels (ground and excited states, g and x) system with a single molecular vibration of frequency ω_v. $\hat{V}_{e-v}$ is the corresponding polaronic-type e-v coupling. $\hat{H}_{NS}$ describes a free electron metal and $\hat{V}_{NS}$ is the molecule-metal electron transfer coupling. $\hat{d}_m^\dagger$ ($\hat{d}_m$) (m=g, x) and $\hat{c}_k^\dagger$ ($\hat{c}_k$) create (annihilate) electrons in the molecular orbitals and the metal, respectively. $\hat{v}^\dagger$ ($\hat{v}$) and$\hat{a}_\alpha^\dagger$ ($\hat{a}_\alpha$) create (annihilate) vibrational excitations and photons in mode α, respectively. Finally, $\hat{D}_M = \hat{d}_g^\dagger \hat{d}_x$ and $\hat{D}_C = \hat{d}_g^\dagger \hat{c}_k$ are respectively intramolecular and charge-transfer electronic de-excitation operators. $\hat{V}_{rad}$, Eq. (8), is the system-radiation field coupling in which the coupling matrix elements $U_{gx,\alpha}^J$ connect the molecular ground state g to electronically excited states x. The channel index $J = C, M$ corresponds to the nature of the excited states x: excited molecular states in channel M and excited metal states in channel C. (We have disregarded a term similar to (8) but with the lower energy state belonging to the pure metal that is associated with light scattering from the bare metal but does not contribute to the interference mechanism discussed below).

As usual, we distinguish between the incoming (occupied) photon mode i and the continuum of accepting (empty) modes $\{f\}$. These coupling elements are assumed to be functions of the vibrational coordinate, described here by their Taylor expansion up to linear term ($J = M, C$)

$$U_{gx,\alpha}^J(\hat{Q}_v) \equiv U_{\alpha,gx}^{J*}(\hat{Q}_v) \approx U_{gx,\alpha}^{J0} + U_{gx,\alpha}^{J1} \hat{Q}_v \tag{9}$$

To account for the observed dependence of the inelastic spectrum on the incident light intensity, we assume that in addition to being scattered, the incident radiation field affects the molecule-metal coupling. This can arise from a field-induced renormalization of the electron transfer coupling $\hat{V}_{NS}$, Eq. (5),[34–36] as well as contributions from molecule to metal charge transfer transitions. In the calculations reported below this is incorporated by an assumed dependence of the self-energies Γ_m ($m = g, x$) on the incident light intensity.

III. THEORETICAL CONSIDERATIONS

Consider first model A (Fig. 3a). Here we assume that Raman scattering is dominated by the intramolecular optical transition and disregard the corresponding contribution of the optical charge transfer coupling V_{rad}^C. This model can show interference between the vibrational and electronic scattering channels, provided that their coupling, Eq (6), is strong enough.

Following the procedure described in Ref. 18 the (normal) Raman scattering flux[37] has the following structure

$$J_{i\to f} = \int_{-\infty}^{+\infty} d(t'-t) \int_{-\infty}^{0} d(t_1-t) \int_{-\infty}^{0} d(t_2-t') \times e^{-i\nu_f(t'-t)} e^{-i\nu_i(t_1-t_2)} \times \left\langle \hat{U}_i(t_2)\hat{D}(t_2)\hat{U}_f(t')\hat{D}^\dagger(t')\hat{U}_f(t)\hat{D}(t)\hat{U}_i(t_1)\hat{D}^\dagger(t_1) \right\rangle \tag{10}$$

in which the operators are summed over all relevant contributions from Eqs. (8) and (9) and where the indices i and f indicate that the corresponding matrix element should be taken with the incident or scattered radiation field modes, respectively. In departure from Ref. [18] we keep only the lowest order (up to 2^{nd}) terms in U^1, as usually done for non-resonant Raman calculations. The calculation proceeds as follows (See the SI for details):

(a) Applying Eq. (10) to model A, yields Eqs. (S2) for the light scattering flux. Expressions (S2b)-(S2e) formally represent interference between vibrational and electronic-Raman/Rayleigh scattering. At the level of the present calculation, fourth order in the coupling to

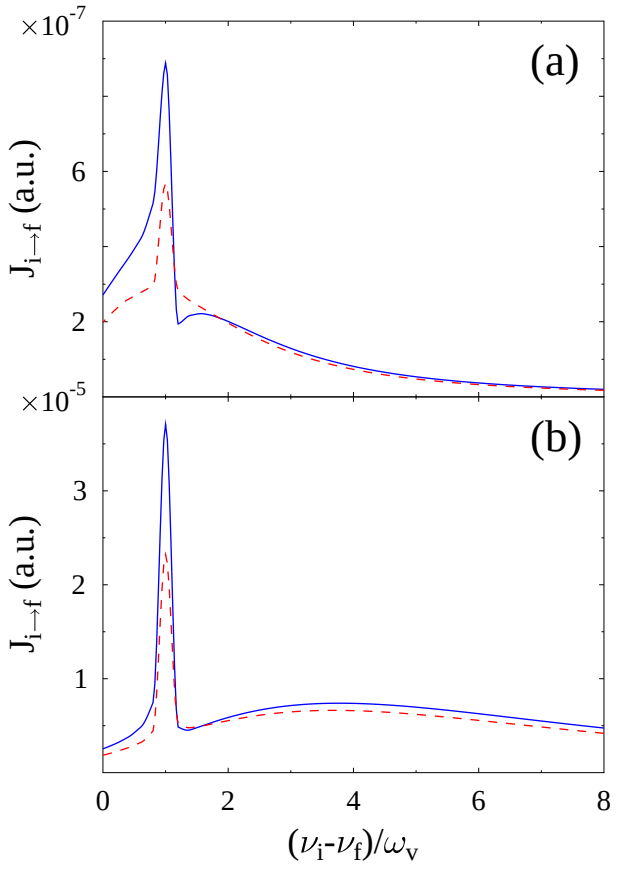

FIG. 4: (Color online) The Raman scattering (full line; blue) evaluated from Eqs. (S10)-(S16), displayed against the Raman shift $\nu_i - \nu_f$. The parameters used are $T = 300$ K, $\varepsilon_g = 0$, $\varepsilon_x = 2$ eV, $\Gamma_g = \Gamma_x = 0.05 + \Gamma^{opt}$ eV with Γ^{opt} being the light induced tunneling rate, $\omega_v = 0.05$ eV, $M_g = 0.02$ eV and $\nu_i = 1$ eV. The red dashed line is the result obtained when the e-v interaction (6) is disregarded. Showan are results for (a) weak ($\Gamma^{opt} = 0.03$ eV, $U^{(0)} = 0.032$ eV, $U^{(1)} = 0.0032$ eV) and (b) strong ($\Gamma^{opt} = 0.3$ eV, $U^{(0)} = 0.1$ eV, $U^{(1)} = 0.01$ eV) incident field.

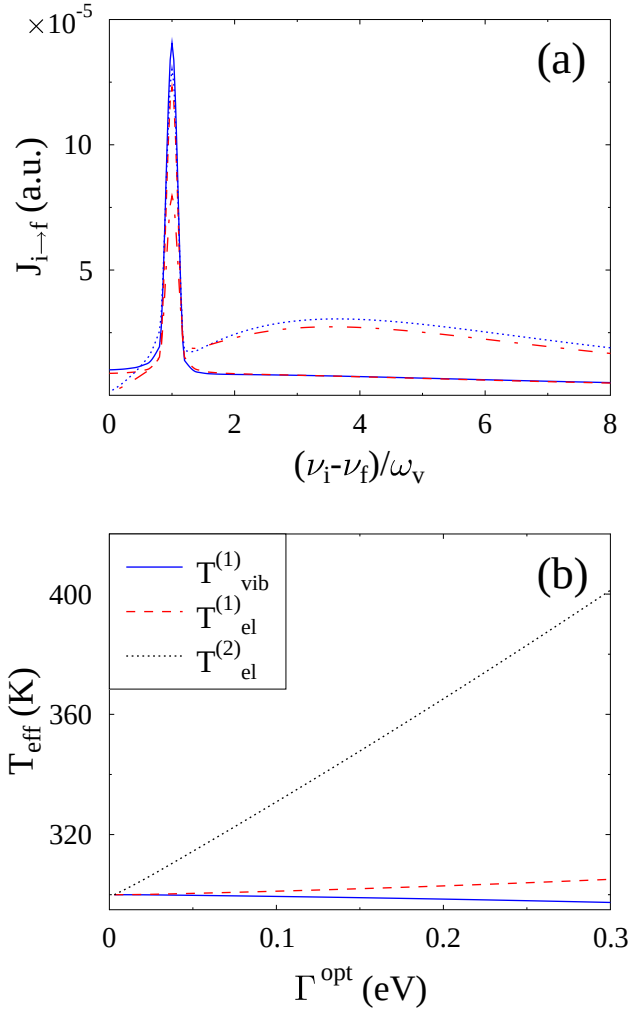

FIG. 5: (Color online) (a) The Raman scattering calculated for parameters of Fig. 4b at $T = 3000$ K (solid and dashed lines) and 30 K (dotted and dash-dotted lines, multiplied by a scale-factor 4). (b) The effective temperature obtained from the Raman spectrum displayed in Fig. 4b.

radiation field, they vanish in the absence of the coupling (6).

(b) The e-v interaction (6) is considered to the lowest order. This introduces an additional term, $\int_c d\tau_v M_g \hat{Q}_v(\tau_v)\hat{n}_g(\tau_v)$, into the correlation functions (S2b)-(S2e), yielding non-vanishing corrections that represent interference between the electronic and vibrational Raman processes. These corrections give non-vanishing contributions to the interference terms, Eqs. (S2b)-(S2e). These can give rise to Fano lineshape in the Raman scattering as shown below.[38]

(c) The light scattering flux including the interference corrections is thus obtained in terms of correlation functions of a system defined by the quadratic Hamiltonian H_0. Consequently, Wick's theorem applies and electronic and vibrational degrees of freedom decouple yielding the final expressions in terms of projections of the electronic and vibrational Green functions, Eqs. (S5)-(S9).

This procedure leads to an explicit expression for the light scattering flux as a sum over several contributions, $J_{i\to f} = J^{(1)}_{i\to f} + J^{(2)}_{i\to f} + J^{(3)}_{i\to f} + J^{(4)}_{i\to f}$, where $J^{(1)}_{i\to f}$ is the electronic Raman flux and $J^{(2)}_{i\to f}$ is the correction to this flux due to the electron-vibration coupling. Similarly $J^{(3)}_{i\to f}$ and $J^{(4)}_{i\to f}$ are respectively the vibrational Raman flux and the correction to this flux associated with the electron-vibration coupling. Explicit expressions for these contributions are given by Eqs. (S10)-(S16).

We have also considered model B as an alternative mechanism for interference. The calculation follows the same steps as in (a) and (c) above, now using both M and C terms in Eq. (8). In this calculation we have restricted our considerations to contributions from the purely intra-

molecular processes ($\hat{D} = \hat{D}_M$ in all four terms in (10)), purely charge-transfer processes ($\hat{D} = \hat{D}_C$ in all terms), and their mixtures (potential source of interference) in which excitation operators at times t_2 and t' are of one kind, while those at times t and t_1 of the other. The final result for the light scattering flux for this model is given by Eqs. (S17)-(S21).

IV. RESULTS

Fig. 4 shows the total Raman scattering signal resulting from a calculation based on model A and on reasonable choice of molecular parameters. The calculation was done on an energy grid spanning the region from -3 to 3 eV with step 10^{-3} eV and the molecular vibration is assumed to equilibrate quickly to the ambient temperature. The following observations can be made:

(a) Interference between electronic and vibrational inelastic scattering routes can indeed lead to a Fano-type scattering spectrum. The electron-vibration coupling (6) is crucial for obtaining this behavior. This is seen in the weak illumination case (Fig. 4a) by comparing the results obtained with and without this coupling.

(b) The asymmetric lineshape that seen in the high incident intensity case (Fig 4b) is not of this origin. In this case the calculation yields Fano-like lineshapes that qualitatively reproduce the experimental behavior also when the coupling (6) is disregarded.

(c) Our analysis thus shows that interference between vibrational and electronic Raman scattering can in principle lead to a characteristic Fano lineshape in Raman scattering from molecules at metal interfaces. The origin of of the present observation appears however to be different, resulting from the Stokes component of the electronic Raman scattering. Indeed, Fig. 5a shows that the asymmetry disappears at high ambient temperatures.

Our calculation also yields the effective (Raman) temperature from the ratio between the S and AS scattering intensities according to[13,17,18] $T^{(1)}_{eff} = \frac{\Delta\nu}{\ln\left(J_{\nu_i\to\nu_i-\Delta\nu}/J_{\nu_i\to\nu_i+\Delta\nu}\right)}$, or fitting the tail of the AS signal to $a\,\Delta\nu/\left(1-\exp[-\Delta\nu/T^{(2)}_{eff}]\right)$, Eq.(S1), where $\Delta\nu \equiv |\nu_i - \nu_f|$ is the Raman shift.[39] The results for the parameters of Fig. 4b are shown in Fig. 5b. In spite of this qualitative agreement with the experimental observation, we note that T_{eff} gives only a rough estimate of system heating. This is indicated here by the different results for T_{el} and the discrepancy between the increased T_{el} and the apparent cooling in T_{vib}, keeping in mind that in fact the oscillator was kept at the ambient temperature in this calculation.

Results of calculations based on Model B are shown in Fig. 6. It shows the Stokes side of the Raman response obtained from this model using the following parameters: $T = 300$ K, $\varepsilon_g = 0$ eV, $\varepsilon_x = 2$ eV, $\omega_v = 0.1$ eV, $\nu_i = 1$ eV, $\Gamma_g = \Gamma_x = 0.15$ eV $+ \Gamma^{opt}$ with $\Gamma^{opt} = 0.1$ eV,

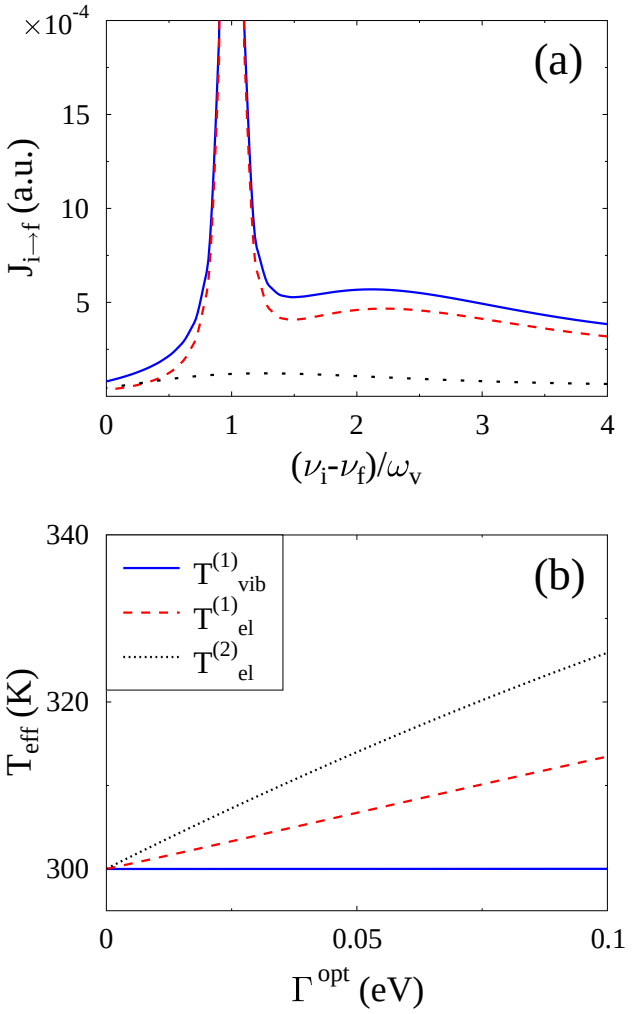

FIG. 6: The Raman scattering signal calculated for model B (see text for parameters). Panel (a) shows the pure-electronic (dotted line, black) and electronic-dressed vibrational Raman (dashed line, red), and their sum (full line, blue). Panel (b) shows the corresponding vibrational and electronic effective temperatures.

$U^{(0)}_{M\alpha} = 0.1$ eV and $U^{(1)}_{M\alpha} = 0.01$ eV ($\alpha = i, f$), and $E_F = 0$. Calculations are performed on an energy grid spanning the region from -5 to 5 eV with step 10^{-3} eV. Asymmetric Raman profiles are seen as before, but again we find (see SI) that while there is some contribution of interference between channels M and C, the main source of lineshape asymmetry originates from the electronic sideband that dresses the Rayleigh and vibrational scattering peaks mainly on their blue side. The "electronic heating" obtained here is stronger than in model A, closer to the magnitude observed experimentally, but the actual numbers should again be considered cautiously.

V. SUMMARY AND CONCLUSIONS

We have observed asymmetric lineshape features in Raman scattering from bipyridyl ethylene molecules adsorbed on gold nanostructures, with the following characteristics: (a) Asymmetry increases with incident light intensity. (b) The vibrational temperature appears not to increase even at the highest intensity used, while the apparent electronic temperature increases by up to ~ 600 K. The Fano-like appearance of these lineshapes suggests the possibly implication of interference between different scattering pathways. Model calculations show that such interference, leading to the observed asymmetry, is indeed possible in systems with strong enough electron-vibrational coupling. Our calculations suggest, however, that the observed lineshape asymmetry is dominated by electronic scattering sidebands that dress the Rayleigh and vibrational scattering peaks, and its dependence on incident light intensity can be explained by an optically induced component in the molecule-metal electron-transfer coupling. This model also yields vibrational and electronic "Raman temperatures" that are consistent with experimental observation, but may reflect the complex nature of the non-equlibrium response rather than the actual temperature. Fano-type interference in Raman scattering has been shown to be a theoretical possibility.

Acknowledgments

AN's research is supported by the Israel and the Binational US-Israel Science Foundations. AN thanks the Theoretical Physics Group at FUB. MG gratefully acknowledges support by the DOE (Early Career Award, DE-SC0006422). The experimental work was carried out at the NSF Center for Chemistry at the Space-Time Limit (CHE-0802913). EH is supported by the Academy of Finland (Decision No. 265502).

[1] M. Moskovits, Rev. Mod. Phys. **57**, 783 (1985).
[2] J. I. Gersten and A. Nitzan, Surface Science **158**, 165 (1985).
[3] J. I. Gersten, Plasmonics **2**, 65 (2007).
[4] J. I. Gersten, R. L. Birke, and J. R. Lombardi, Phys. Rev. Lett. **43**, 147 (1979).
[5] A. Otto, I. Mrozek, H. Grabhorn, and W. Akemann, Journal of Physics: Condensed Matter **4**, 1143 (1992).
[6] A. Otto and M. Futamata, *Surface-Enhanced Raman Scattering: Physics and Applications* (Springer, 2006), vol. 103, chap. Electronic Mechanism of SERS, pp. 143–182.
[7] S. M. Morton, D. W. Silverstein, and L. Jensen, Chemical Reviews **111**, 3962 (2011).
[8] S. W. Wu, G. V. Nazin, and W. Ho, Phys. Rev. B **77**, 205430 (2008).
[9] Z. Ioffe, T. Shamai, A. Ophir, G. Noy, I. Yutsis, K. Kfir, O. Cheshnovsky, and Y. Selzer, Nature Nanotechnology **3**, 727 (2008).
[10] D. R. Ward, N. J. Halas, J. W. Ciszek, J. M. Tour, Y. Wu, P. Nordlander, and D. Natelson, Nano Lett. **8**, 919 (2008).
[11] Z. Liu, S.-Y. Ding, Z.-B. Chen, X. Wang, J.-H. Tian, J. R. Anema, X.-S. Zhou, D.-Y. Wu, B.-W. Mao, X. Xu, et al., Nat Commun **2**, 305 (2011).
[12] T. Shamai and Y. Selzer, Chem. Soc. Rev. **40**, 2293 (2011).
[13] D. R. Ward, D. A. Corley, J. M. Tour, and D. Natelson, Nature Nanotechnology **6**, 33 (2011).
[14] T. Konishi, M. Kiguchi, M. Takase, F. Nagasawa, H. Nabika, K. Ikeda, K. Uosaki, K. Ueno, H. Misawa, and K. Murakoshi, Journal of the American Chemical Society **135**, 1009 (2013).
[15] D. Natelson, Y. Li, and J. B. Herzog, Phys. Chem. Chem. Phys. **15**, 5262 (2013).
[16] M. Galperin and A. Nitzan, Phys. Chem. Chem. Phys. **14**, 9421 (2012).
[17] M. Galperin, M. A. Ratner, and A. Nitzan, Nano Lett. **9**, 758 (2009).
[18] M. Galperin, M. A. Ratner, and A. Nitzan, J. Chem. Phys. **130**, 144109 (2009).
[19] T.-H. Park and M. Galperin, Europhys. Lett. **95**, 27001 (2011).
[20] T.-H. Park and M. Galperin, Phys. Rev. B **84**, 075447 (2011).
[21] M. Galperin and A. Nitzan, J. Phys. Chem. Lett. **2**, 2110 (2011).
[22] M. Galperin and A. Nitzan, Phys. Rev. B **84**, 195325 (2011).
[23] F. Mirjani, J. M. Thijssen, and M. A. Ratner, The Journal of Physical Chemistry C **116**, 23120 (2012).
[24] M. Oren, M. Galperin, and A. Nitzan, Phys. Rev. B **85**, 115435 (2012).
[25] T.-H. Park and M. Galperin, Phys. Scr. T **151**, 014038 (2012).
[26] K. Kaasbjerg, T. Novotný, and A. Nitzan, Phys. Rev. B **88**, 201405 (2013).
[27] A. J. White, S. Tretiak, and M. Galperin, Nano Letters **14**, 699 (2014).
[28] E. Burstein, Y. Chen, C. Chen, S. Lundquist, and E. Tosatti, Solid State Communications **29**, 567 (1979).
[29] W. Akemann and A. Otto, Surface Science **307-309, Part B**, 1071 (1994).
[30] T. Itoh, V. Biju, M. Ishikawa, Y. Kikkawa, K. Hashimoto, A. Ikehata, and Y. Ozaki, The Journal of Chemical Physics **124**, 134708 (2006).
[31] R. R. Frontiera, N. L. Gruenke, and R. P. V. Duyne, Nano Lett. **12**, 5989 (2012).
[32] S. Marhaba, G. Bachelier, C. Bonnet, M. Broyer, E. Cottancin, N. Grillet, J. Lerm, J.-L. Vialle, and M. Pellarin, The Journal of Physical Chemistry C **113**, 4349 (2009).
[33] S. Yampolsky, D. A. Fishman, S. Dey, E. Hulkko, M. Banik, E. O. Potma, and V. A. Apkarian, Nat. Photon. **8**, 650 (2014).
[34] S. D. Ganichev, E. Ziemann, T. Gleim, W. Prettl, I. N. Yassievich, V. I. Perel, I. Wilke, and E. E. Haller, Phys. Rev. Lett. **80**, 2409 (1998).

[35] D. R. Ward, F. Huser, F. Pauly, J. C. Cuevas, and D. Natelson, Nature Nano **5**, 732 (2010).

[36] M. Vadai, N. Nachman, M. Ben-Zion, M. Brkle, F. Pauly, J. C. Cuevas, and Y. Selzer, The Journal of Physical Chemistry Letters **4**, 2811 (2013).

[37] We limit consideration to unbiased or weakly biased junctions, where only normal Raman scattering, where the initial electronic state is the ground state of the molecule, can take place.

[38] A closer look at the details of these corrections reveals that corrections to (S2b)-(S2c) from projections (e)-(h) of Fig. S5 and corrections to (S2d)-(S2e) from projections (a)-(d) of Fig. S5 represent renormalization of the electronic Raman signal due to e-v interaction. These terms dominate the resulting Fano resonance that is seen in the calculated Raman scattering at low incident light intensity (inset to Fig. 3a). Corrections to (S2b)-(S2c) from projections (a)-(d) of Fig. S5 and corrections to (S2d)-(S2e) from projections (e)-(h) of Fig. S5 lead to renormalization of the vibrational Raman scattering and are included as well in the calculations reported here.

[39] For $T_{eff}^{(1)}$ we have arbitrarily assigned the vibrational Raman temperature to the value calculated at $\Delta\nu = \omega_v$ and the electronic Raman temperature to that obtained at $\Delta\nu = 2\omega_v$.